NEXRES 2 (2025) 100996

Contents lists available at ScienceDirect

Next Research

journal homepage: www.elsevier.com/locate/nexres

Photo-activated antibacterial effect of bimetallic nanocomposite grafted on modified PET substrate

Veronika Lacmanová [a], Radek Ostruszka [b], Martin Petr [c], Petr Slepička [a], Filip Průša [d], Ondřej Kvítek [a], Anna Kutová [a], Alena Řezníčková [a,*], Karolína Šišková [b,*]

[a] Department of Solid State Engineering, University of Chemistry and Technology Prague, 166 28 Prague, Czech Republic
[b] Department of Experimental Physics, Faculty of Science, Palacký University Olomouc, 17. listopadu 12, 779 00 Olomouc, Czech Republic
[c] CATRIN, Palacký University Olomouc, Šlechtitelů 27, 779 00 Olomouc, Czech Republic
[d] Department of Metals and Corrosion Engineering, University of Chemistry and Technology Prague, 166 28 Prague, Czech Republic

ARTICLE INFO

Keywords:
Au nanostructures
Iron oxide particles
Polymer substrate
Light-induced process
E. coli
Antibacterial surface

ABSTRACT

The current work aims to test (a) possibility of grafting (via a dithiol linker) and (b) applicability of bimetallic nanocomposites (developed in our recent work) as photo-stimulated antibacterial coatings. Therefore, bimetallic nanocomposites, containing (i) Au nanostructures (AuNS) embedded in a protein matrix and (ii) superparamagnetic iron oxide nanoparticles (SPION) attached to the same protein scaffold (bovine serum albumin), were grafted on a flexible and UVA-transparent substrate (PET, polyethylene terephthalate). Plasma-treatment and dithiol surface modification of PET were successfully employed to increase the probability of bimetallic nanocomposite attachment. It was evidenced by XPS (X-ray photoelectron spectroscopy) that albeit AuNS are bound up in the protein by Au-S linkage, grafting on plasma-treated surface-modified PET is enabled due to the same bonding type. The final system (Au-BSA-SPION@pl-BPD-PET) revealed no antibacterial activity against *Escherichia coli* under ambient conditions as it was expected. However, when photo-activated by UVA radiation (365 nm), applied for a short period (5 min), its antibacterial activity was switched on. Bimetallic nanocomposite can be thus considered as a photo-switchable functional surface coating of PET. To the best of our knowledge, it is the very first photo-stimulated antibacterial surface coating that is based on bimetallic AuNS-SPION nanocomposites.

1. Introduction

Bacteria resistance against antibiotics as well as against selected nanoparticles, such as silver for instance, represents a threat to human society in many countries and causes serious public health issues throughout the world [1,2]. As an example, monitoring water quality and preventing contamination by fecal bacteria are critically important for public health. Another issue is represented by the accumulation of antibiotics in the environment, consequently leading to development of bacteria resistance. To solve these issues, new antimicrobial agents (including nanostructures, antimicrobial peptides, and/or quaternary ammonium compounds) and novel antibiotic drugs have been designed already. As one alternative, efficient antibacterial properties of nanostructured materials consisting of Ag and/or Cu have been frequently chosen and are well known for decades. Antimicrobial activity relies on the release of metal cations, which, unfortunately, can adversely affect various biological components [3–6]. Therefore, there is a growing trend to avoid the usage of silver and/or copper in nanostructured forms. Alternatively, an emerging approach for combating antibiotic accumulation in the environment involves antibacterial activity that is triggered by an external stimulus.

There are different kinds of the external stimulus that switches the antibacterial properties of a system such as for instance: tailored supramolecular interactions, denaturant induced folding/unfolding of natural enzymes, temperature-change, pH-change, photon impact etc. [1,7–9,10]. Among the external stimuli, light/radiation is the most perspective one because it avoids contamination of the sample (being thus non-invasive in this sense). Moreover, it offers relatively high spatiotemporal resolution, its wavelength and intensity can be precisely controlled [1,11]. Different regions of electromagnetic radiation serving

* Corresponding authors at: Department of Experimental Physics, Faculty of Science, Palacký University Olomouc, 17. Listopadu 12, 779 00 Olomouc, Czech Republic.
E-mail addresses: alena.reznickova@vscht.cz (A. Řezníčková), karolina.siskova@upol.cz (K. Šišková).

https://doi.org/10.1016/j.nexres.2025.100996
Received 17 July 2025; Received in revised form 21 October 2025; Accepted 28 October 2025
Available online 29 October 2025

as external stimuli and boosting antibacterial properties have been exploited in conjunction with nanomaterials and polymers already, such as near infrared (NIR) [12,13], visible (Vis) [14,15], and/or UV radiation [16]. There are advantages and disadvantages connected to each spectral region. For instance, it is well-known that NIR radiation can penetrate deeper than Vis and/or UV into the matter, however, it provides the least energy from the selected spectral regions and, consequently, it may be insufficient for photo-induced reactions. On the contrary, UV radiation might be considered a little bit problematic due its higher energy and negative impact on living organisms. Nevertheless, the general term of UV radiation includes subregions (UVA, UVB, UVC) that substantially differ by their impact on living systems. UVA radiation is the mildest one from UV region (spanning from 315 nm to 400 nm) and represents around 90 % of sunlight on the earth.

Among light-responsive materials, metal-based nanostructures with unique tuneable optical properties have attracted enormous attention in various fields of research [17]. The usage of photo-activation is quite frequent for semiconducting materials, such as TiO_2, ZnO, and/or Fe_xO_y containing nanocomposites [6,18,19]. In this case of semiconductive metal-oxide nanostructures, the photoactivation causes reactive oxygen species generation. This can be effectively exploited for combating bacteria. Since radiation of a specific wavelength is used as a trigger, it is easier to control and suppress bacterial resistance.

Recently, bimetallic nanocomposite consisting of (i) superparamagnetic iron oxide nanoparticles (SPION) attached to a protein, and (ii) Au nanostructures (AuNS) embedded in the same protein (bovine serum albumin), has been proven to produce hydroxyl radicals in aqueous environment upon UVA light irradiation [20]. Generally, hydroxyl radicals are considered as efficient agents against bacteria. Particularly, they are very efficient in fighting against *E. coli* as published recently [21]. Therefore, the current work aims to explore if bimetallic nanocomposites (Au-BSA-SPION) prepared by green chemistry approach [20,22,23] can cause photo-induced antibacterial effect or not.

For an easier handling and inspired by antifouling coatings used in medical devices for instance [24], bimetallic nanocomposites need to be grafted on a flexible and UVA-transparent substrate. In this context, polyethylene terephthalate (PET) serves as a suitable substrate owing to its excellent flexibility, transparency to UVA [25], and ease of surface modifications [26–29]. Prior to any nanostructure grafting, PET surface must undergo sequential surface modification through plasma treatment followed by functionalization with 4,4′-biphenyl-dithiol (BPD), as demonstrated in previous studies [27–29] involving the immobilization of various noble metal nanoparticles. The primary concern is whether the bimetallic nanocomposites (Au–BSA–SPION) can effectively bind to BPD through Au–S linkages, given that the Au–S interaction has already been utilized for anchoring the Au nanostructures onto the protein scaffold [20]. Therefore, the present work can serve as a direct proof of two concepts: (a) possibility of Au-BSA-SPION grafting on modified polymeric substrate and (b) demonstration of photo-switchable antibacterial properties of the newly formed final system (Au-BSA-SPION@pl-BPD-PET) against *E. coli*.

2. Experimental part

2.1. Materials for bimetallic nanocomposite synthesis

Bovine serum albumin (BSA; >98 %), gold (III) chloride trihydrate ($HAuCl_4{\cdot}3H_2O$; ≥99.9 %), iron (III) chloride hexahydrate ($FeCl_3{\cdot}6H_2O$; ≥99 %), and sodium hydroxide (NaOH; ≥98.0 %) were purchased from Sigma-Aldrich (St Louis, MO, USA) and used as received (without any further purification). Hydrochloric acid (35 %) was purchased from Penta s.r.o. (Prague, Czech Republic). Deionized (DI) water prepared by purging Milli-Q purified water (Millipore Corp., Bedford, MA, USA) was used for nanocomposites synthesis.

2.2. PET substrate modification

Polyethylene terephthalate thin foil (PET, $\rho = 1.3\ g{\cdot}cm^{-3}$, thickness 23 μm, Goodfellow Ltd., UK) was selected for the study. Firstly, samples were activated in DC Ar^+ plasma on Balzers SCD 050 device (BalTec AG, CH): exposure duration 120 s, discharge power 8.3 W, and pressure of 10 Pa. Secondly, the samples were immersed into methanol-based solution of biphenyl-4,4′-dithiol (BPD; $c = 1{\bullet}10^{-3}\ mol{\cdot}l^{-1}$; Sigma-Aldrich Corp., US) for 24 h.

2.3. Bimetallic nanocomposites synthesis and purification

Au-BSA-SPION nanocomposite were prepared by the procedure described in [23]. Briefly, $FeCl_3{\cdot}6H_2O$ (200 μL, 0.1 M) was introduced into a microcentrifuge tube. Subsequently, BSA solution (1 mL, 66.43 $mg{\cdot}mL^{-1}$) was slowly added in two equal portions with constant stirring using a pipette. The reaction mixture was then vortexed at 3000 rpm. Five minutes later, NaOH (57.5 μL, 1 M) was rapidly introduced and the reaction mixture was immediately vortexed. Ten minutes later, $HAuCl_4$ (800 μL, 25 mM) was slowly added under constant stirring. The tube content was swirled in the vortex, and five minutes later, additional NaOH (142.5 μL, 1 M) was quickly introduced into the reaction solution. Then, the tube content was vortexed for the last time. Subsequently, the microcentrifuge tube was placed in a dry bath incubator maintained at 50 °C and incubated for 22.5 h. The whole procedure is schematically depicted in Scheme 1.

After maturation, the sample was dialyzed with a 14 kDa cut-off dialysis membrane (regenerated cellulose, Membra-Cel™) against deionized water. Dialysis was performed against deionized water at room temperature (22 °C) for 5 h (deionized water was changed after 30 min, 45 min, 60 min, and 75 min). The as-prepared sample is of orange-brown colour without any aggregate or agglomerate visible to the naked eye. Main characteristics of Au-BSA-SPION can be found out in refs [22, 23]. Nevertheless, representative high-resolution transmission electron microscopic (HR-TEM) image, energy-dispersive spectroscopic (EDS) mapping, Mössbauer spectrum, X-ray diffraction pattern (XRD) and X-ray photoelectron spectroscopic (XPS) investigations (Au-BSA-SPION is drop-casted on Si wafer) are shown in Figure SI-1.

2.4. Final system fabrication

The modified PET substrates were transferred into Au-BSA-SPION nanocomposite aqueous solution (described in the previous subsection) where they were kept for 24 h (based on the previous experience with nanoparticles grafting [27–29]; note that shorter times of applied soaking did not provide statistically significant antibacterial effect). After taking the samples out from the bimetallic nanocomposite solution, they were washed out and dried in N_2 stream. The final system (Au-BSA-SPION@pl-BPD-PET) was prepared and stored under laboratory conditions.

2.5. Analytical methods

The XPS measurements were performed on a Nexsa G2 XPS system (Thermo Fisher Scientific) equipped with a monochromatic Al-Kα source and photon energy of 1486.7 eV. The spectra were recorded at two

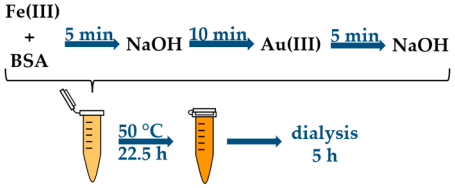

Scheme 1. Depiction of bimetallic nanocomposite synthesis.

angles: 0° (i.e., normal to the surface; providing general sample composition below the surface) and 81° (angle considered from the normal; more information provided directly from the most upper surface layers), under vacuum (1.6×10^{-9} mbar), and at a controlled ambient temperature of 20 °C. Charge neutralization techniques were systematically switched on during the measurement. Spectral analysis and data interpretation were conducted using Avantage software version 6.5.1 provided by Thermo Fisher Scientific.

Ultraviolet-visible (UV–vis) spectroscopy was used to confirm the presence of Au nanostructures on plasma treated and BPD-modified PET. Absorption spectra were evaluated using a Lambda 25 spectrophotometer (PerkinElmer Inc., US) in the spectral range of 400 to 600 nm, scan speed 240 nm·min^{-1} and step of 1 nm. The reference spectrum of pristine PET was subtracted from the collected spectrum of nanostructured PET. The optical absorption error values were lower than 1.5 %.

Infrared spectroscopy analysis was performed by a Fourier-transform infrared (FTIR) spectrometer Nicolet iS5 (Fisher Scientific) with a diamond crystal iD7 ATR accessory. The spectra were obtained as an average from 128 measurement cycles in the spectral range of 1800–600 cm^{-1} with the data interval of 0.964 cm^{-1}.

Static water contact angle (WCA) of distilled water, characterizing chemical and morphological differentiation. Each modification step was evaluated under laboratory conditions using four samples and at ten measurement points with a DSA 100 goniometer (KRÜSS GmbH, DE). Water droplets of (2.0 ± 0.2) µl were dispensed onto the selected sample surfaces for contact angle measurements. WCA values were determined by the ADVANCE software.

Scanning electron microscopy (SEM, Lyra dual beam microscope, Tescan a. s., CZ) was applied for evaluation of surface morphology of pristine PET, plasma treated PET, PET modified with BPD and subsequently with Au-BSA-SPION nanocomposites. SEM analysis was performed in the secondary electron (SE) imaging mode with accelerating voltage of 5 kV. The magnification of the presented SEM images is 100,000 × with 2 × 2 µm^2 scan size. To prevent surface charging, samples were attached to the holder with carbon conductive tape and coated with 10 nm thick carbon layer. The carbon layer was prepared by flash evaporation method using sputtering device Balzers SCD 050 device (BalTec AG, CH).

Atomic force microscope Dimension ICON (AFM, Bruker Corp., US) was employed to investigate the surface morphology and roughness of the prepared samples at nanometre level. AFM analysis was performed with ScanAsyst mode in the air using a silicon tip on a nitride cantilever with a spring constant of 0.4 N·m^{-1}. The acquired data were processed by NanoScope Analysis software to obtain the average surface roughness values (*Ra*). The size of the scans was 300 × 300 nm^2.

2.6. Testing of antibacterial effect

The antibacterial effect of the Au-BSA-SPION nanocomposites grafted on plasma treated surface-modified PET was measured using the drop plate method. The measurement was carried out using the gram-negative bacteria (G-) *E. coli* (*E. coli*; DBM 3138). One colony was used to prepare the inoculum, which was transferred sterilely with a bacteriological loop in 25 ml (*E. coli*) of Luria-Bertani (LB) liquid medium. Subsequently, the inocula were incubated overnight on an orbital shaker at 37 °C. Next, they were diluted in sterile phosphate buffered saline (PBS) to final concentration of approx.2×10^3 (*E. coli*) per mL. 200 µL drop of diluted bacterial suspension was deposited onto the samples' surface and left for 2 h at room temperature. Then, five drops (25 µL) of bacterial suspension from each sample surface were placed on plate count agar (PCA, Oxoid, containing tryptone 5 g·L^{-1}, yeast extract 2.5 g·L^{-1}, glucose 1 g·L^{-1}, agar 15 g·L^{-1}) culture dish. Cultivation was carried out overnight at room temperature. The next day, the grown colony-forming units (CFU) were counted. All experiments were performed under sterile conditions.

All antibacterial tests were carried out in three independent measurements (i.e. three samples), each of them including five repetitions (i.e., five drops for CFU counting for one measurement). To show the differences between the samples and pristine glass, the two-sample *t*-test assuming equal variance (Excel, Microsoft Office, US) was done.

3. Results and discussion

Bimetallic nanocomposites prepared according to the previous work [22,23] were characterized by several physicochemical experimental techniques as detailed in the Supporting information (Figure SI-1) for completeness. The main characteristics of bimetallic nanocomposites were proven, such as: nanostructure sizes below 5 nm in diameter (Figure SI-1A), close vicinity of Au and Fe nanostructures (Figure SI-1B), colocalization of Au and S elements (Figure SI-1C), colocalization of Fe and O elements (Figure SI-1D), elemental composition from the selected area (Figure SI-1E), content of Au (0) and Au-S bond evidenced by XPS (Figure SI-1F), presence of superparamagnetic ferric oxide particles according to Mössbauer spectroscopy (Figure SI-1 G), and representative XRD pattern (Figure SI-1H) confirming amorphous character of bimetallic nanocomposites. Then, the possibility of bimetallic nanocomposite attachment to the chosen flexible, light, and UVA-transparent substrate (PET) could be tested. This represents the prerequisite for nanocomposite serving as potential antibacterial coating. Prior to the bimetallic nanocomposite grafting, plasma treatment and BPD-modification of PET substrates have been performed as inspired by the previous works [26–28]. In the following text, we are going to focus mainly on the final system, i.e. bimetallic nanocomposites grafted on modified PET substrate, denoted as Au-BSA-SPION@pl-BPD-PET.

3.1. Surface properties of Au-BSA-SPION@pl-BPD-PET in comparison to pristine and/or modified PET substrates

PET substrates exhibit slight hydrophobicity (82.7 ± 1.8°), which increases further (96.2 ± 2.3°) following plasma treatment and subsequent surface modification with biphenyl dithiol (BPD) as evidenced by the water contact angle (WCA) measurements shown in Fig. 1.

When bimetallic nanocomposites generated in an aqueous solution are allowed to graft to the surface-modified PET substrates, the WCA changes to 63.5 ± 1.3° – Fig. 1. Our WCA results correlate well with those previously published, dealing with either plasma-treatment procedure of selected polymers [26], or nanoparticles grafted on plasma-treated and surface-modified PET substrates [29]. Similar values of WCA (between 64–69°) were obtained when metal nanoparticles of different origins (electrochemically/chemically prepared) were grafted on PET substrates [29]. It thus reports indirectly about successful bimetallic nanocomposites grafting on PET substrate.

Another indirect proof of PET surface modifications and bimetallic nanocomposite grafting is obtained by SEM imaging (Figure SI-2), where almost-spherical nanoobjects of sizes around 50 nm as well as irregularly shaped clumps of these nanoobjects can be recognized (Figure SI-2C).

AFM revealed changes in surface roughness values (Ra) due to surface modification induced by plasma treatment and BPD attachment (Fig. 2): while PET substrate manifested itself by Ra = 0.5 nm, plasma-treated and BPD-modified PET substrate by Ra = 1.7 nm. For the bimetallic nanocomposite grafted onto the modified PET substrate, the surface roughness increased further to Ra = 3.7 nm, providing additional evidence of successful nanocomposite grafting.

When compared with scientific literature (e.g., [27,28]), PET surface roughness augments from Ra = 0.5 nm (smooth surface) to Ra = 1.7 nm for plasma treated and BPD-modified PET. Indeed, the disruption of macromolecular chains in the upper layer of PET is the reason for the observed increase in surface roughness [29]. A further augmentation of Ra values revealed for the final system (bimetallic nanocomposites grafted on plasma-treated and BPD-modified PET substrate), 3.7 nm (Fig. 2C). It lies approximately in the middle of the Ra values obtained

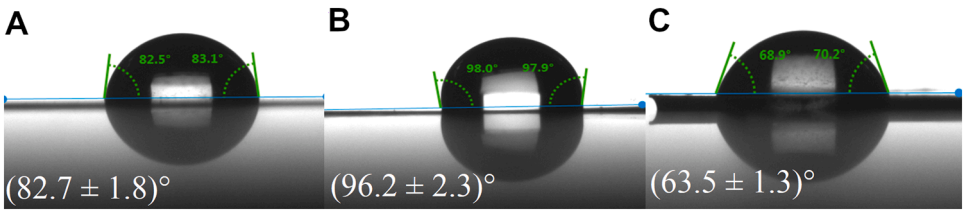

Fig. 1. Representative results of water contact angle (WCA) measurements for pristine PET substrate (A), plasma-treated and BPD-modified PET substrate (B), and bimetallic nanocomposites grafted on plasma-treated surface-modified PET (C).

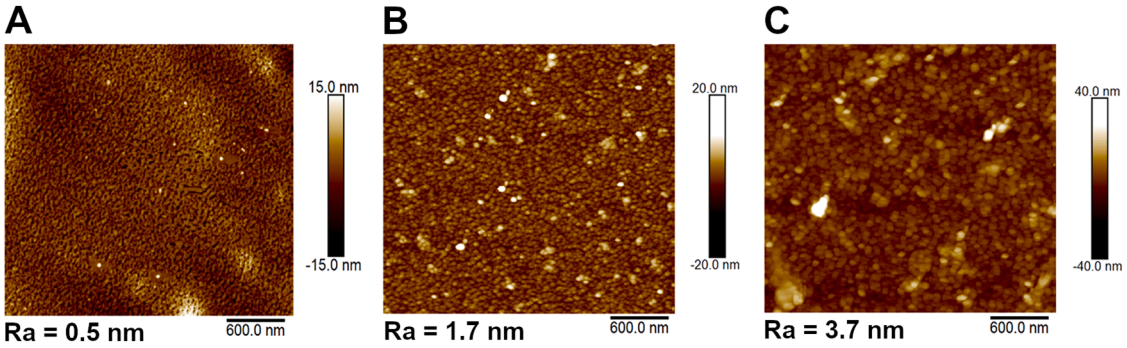

Fig. 2. Atomic force microscopic images of PET substrate (A), plasma-treated and BPD-modified PET substrate (B), and bimetallic nanocomposites grafted on plasma-treated surface-modified PET (C).

for a comparable system: AgNPs of different origins (i.e., electro-/-chemically and physically prepared) grafted on plasma-treated and BPD-modified PET substrates [29].

3.2. *Spectroscopic characterization of Au-BSA-SPION@pl-BPD-PET*

The UV–vis and IR absorption spectra of surface modified PET substrate with and without grafted bimetallic nanocomposite did not show any significant differences (Figures SI-3 and SI-4). On the contrary, XPS spectroscopy as a surface specific analytical method (investigating roughly top 10 nm of the surface) gave direct evidence of a successful grafting of bimetallic nanocomposites since Fe and Au signals were clearly detected and changes in C, O, N, S contents were also observed: the atomic percentage of these elements derived from XPS survey scans at two different angles, 0° (i.e., perpendicular to the substrate surface) and 81° (considered from the vertical) provided information about the composition of subsurface vs top layers, respectively - Table 1.

Considering the atomic percentage of elemental contents derived from XPS measurements (Table 1), iron predominates over gold in the final system. Looking at detailed XPS scans and fitting the signals of the selected elements (Au 4f, S 2p, N 1 s, and C 1 s) - Fig. 3, one can distinguish obvious chemical composition differences between subsurface and top layers.

Table 1
Comparison of the elemental composition of Au-BSA-SPION@pl-BPD-PET and of pl-BPD-PET, determined for subsurface (0°) vs. top (81°) layers by XPS measurements.

Element	Au-BSA-SPION@pl-BPD-PET		pl-BPD-PET substrate	
	Subsurface layers [Atomic %]	Top layers [Atomic %]	Subsurface layers [Atomic %]	Top layers [Atomic %]
C 1s	66.0	67.2	70.2	70.8
O 1s	22.3	22.1	21.1	22.5
N 1s	8.1	7.2	1.4	0.9
Fe 2p	2.1	2.1	-	-
S 2p	1.5	1.4	0.4	0.6
Au 4f	<0.1	<0.1	-	-

It should be noted that Au (0) content derived from detailed XPS Au 4f signals in bimetallic nanocomposites *per se* (i.e., prior to any grafting) is around 64.5 %, while Au-S represents the rest of the signal (35.5 %) - Figure SI-1F (measured in subsurface layers). On the contrary, the grafted bimetallic nanocomposite contains only approx. 35 % of Au (0) and approx. 65 % of Au-S (denoted as Au(δ+)) - Fig. 3A. Therefore, from the direct comparison of Au (0) vs Au-S in bimetallic nanocomposites prior and after grafting to modified PET substrate (measured in subsurface layers), one can assume that bimetallic nanocomposite interacts with modified PET substrate through gold atoms; indeed, almost one-half of gold atoms in the oxidation state of 0 are exploited for the interaction with sulphur of BPD. By the act of bonding to sulphur, Au (0) is changed/oxidized to Au (δ+).

Furthermore, the content of Au (0) at top layers decreased by approx. 5 % with a simultaneous increase of Au (δ+), again by approx. 5 % as can be derived from the comparison of curves in Fig. 3A. It means that Au (0) is partially oxidized at top layers. This is further supported by a detailed investigation of S 2p region: approx. 8 % of Au-S and approx. 78 % of R-SH in subsurface layers, whereas almost 20 % of Au-S and around 65 % of R-SH at top layers (Fig. 3B). The increased content of Au-S at the expense of R-SH at top layers clearly shows that Au (stemming from the bimetallic nanocomposite) is bound to sulfur of BPD (molecular modifier of PET substrate). It should be also reminded that a nonnegligible portion of Au-S bonds originates from the bimetallic nanocomposite itself (Figure SI-1F), where cysteine residues are bound with the edge atoms of Au nanoclusters. The discrepancy between the exact percentage changes (5 % in Au 4f region vs 12 % in S 2p region) may be caused by uneven distribution of nanocomposites grafted on plasma-treated and BPD-modified PET substrates as well as by a further component in S 2p region (assigned to sulphites/sulphates).

Considering organic part of the nanocomposite grafted on modified PET substrate, there are distinct differences in N 1 s and C 1 s XPS signals between subsurface and top layers. N 1 s region in subsurface layers (Fig. 3C) evidences the presence of amidic bond and ammonium, both functionalities stemming from the protein matrix of the grafted nanocomposite (note: PET substrate, neither its molecular modifier, BPD, do not contain any nitrogen within their structures). In addition to these two functionalities, amine (8 %) is detected at the top layers of the final

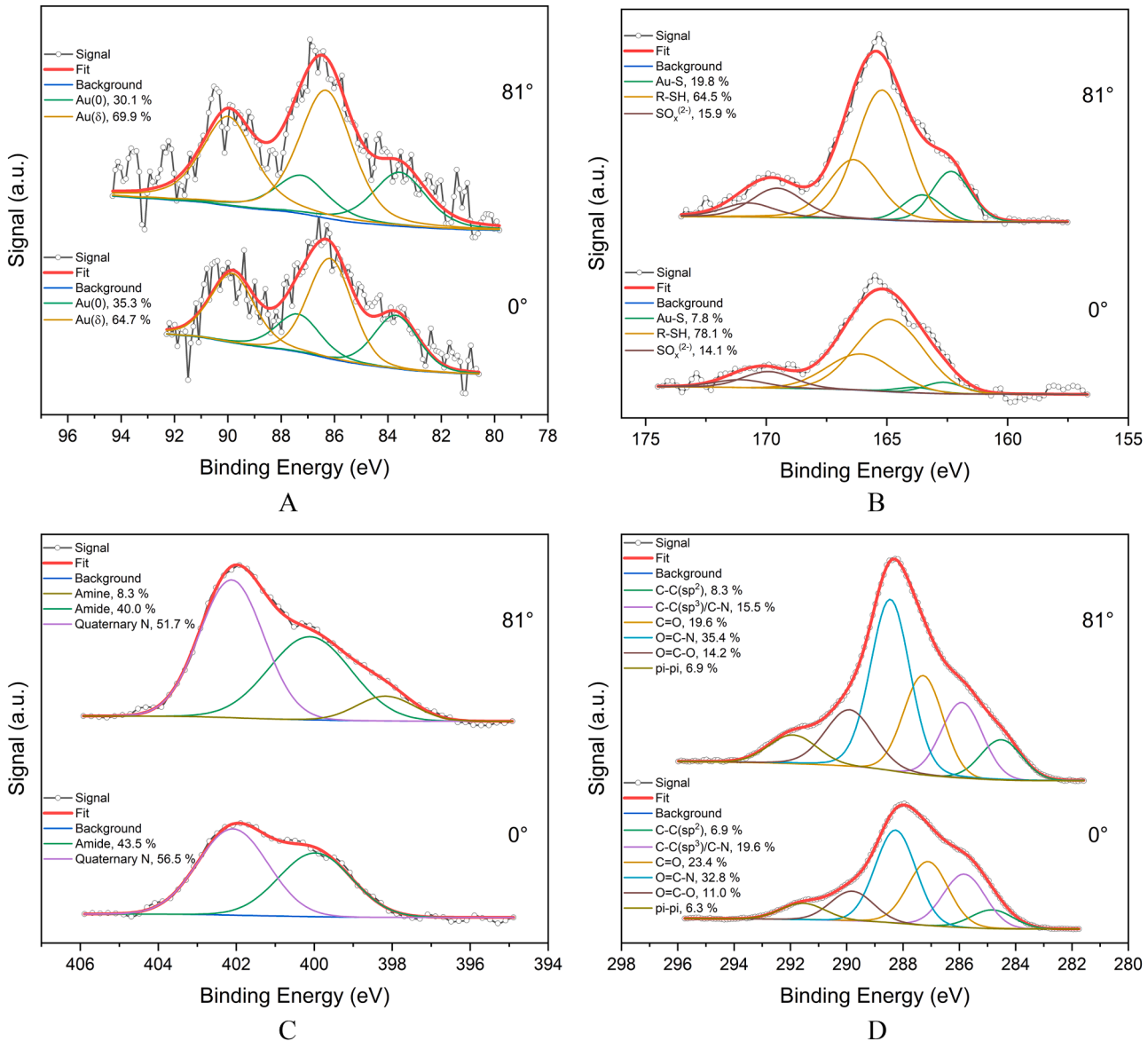

Fig. 3. Detailed XPS signals fitting in: (A) Au 4f, (B) S 2p, (C) N 1 s, and (D) C 1 s regions for the data recorded at 0° (subsurface) and 81° (top layers).

system (Fig. 3C). This observation may be attributed most probably to conformational changes of the protein. This hypothesis is further corroborated by changes revealed in C 1 s region of detailed XPS signal when going from subsurface to top layers (Fig. 3D). Particularly: $O = C$—O increased by 3.2 %, $O = C$—N by 2.6 %, C—C (sp^2) by 1.3 %, and л-л by 0.6 % at the expense of C—C (sp^3) and $C = O$ that decreased by 4.1 % and by 3.8 %, respectively. The assignment of peaks within Au 4f, S 3p, N 1 s, and C 1 s regions corresponds well to the literature [30–32]. Indeed, Au and SPION nanostructures are embedded in the protein matrix and in the process of grafting to the modified substrate (via Au-S bonds), the protein matrix is forced to change its conformation. Therefore, XPS signals of N and C in subsurface vs top layers of the final system can differ.

Comparing XPS signals of the dispersed nanocomposite in solution with that of the nanocomposite grafted state on PET, the following can be summarized: the dispersed Au-BSA-SPION contains Au nanoclusters predominantly in the Au (0) state (≈65 %), embedded in the protein scaffold, while SPION are stably coordinated to BSA residues. Upon grafting to the BPD-modified PET substrate, however, XPS analysis evidences a pronounced decrease of Au (0) to ≈35 % with a concomitant increase of Au(δ+). This observation directly supports the formation of Au–S covalent bonds with the PET surface modifier, which leads to a partial oxidation of gold atoms. In addition, the N 1 s and C 1 s regions reveal conformational changes in the protein matrix upon immobilization, consistent with rearrangements not observed in the dispersed state. The comparison thus demonstrates that the interaction with the polymer substrate is dominated by Au–S anchoring, while SPION remain more exposed to the environment, providing a mechanistic explanation for the surface functionality of the final grafted system.

Based on the above discussed observations derived from XPS, it can be concluded that our bimetallic nanocomposite is grafted to the modified PET substrate via Au-S covalent bond (however, not all AuNCs are accessible, some of them are hidden within protein matrix) and SPION (mostly bonded to N-terminal region of the protein as revealed in our recent work [20]) is exposed to the ambient environment - Fig. 4.

3.3. *Antibacterial properties of Au-BSA-SPION@pl-BPD-PET*

Antibacterial effect of Au-BSA-SPION@pl-BPD-PET has been tested against *E. coli* and the results are shown in Fig. 5. It should be reminded that due to a good wettability as well as absence of any sharp objects (proven in Section 3.1) on the final surface coating, a successful

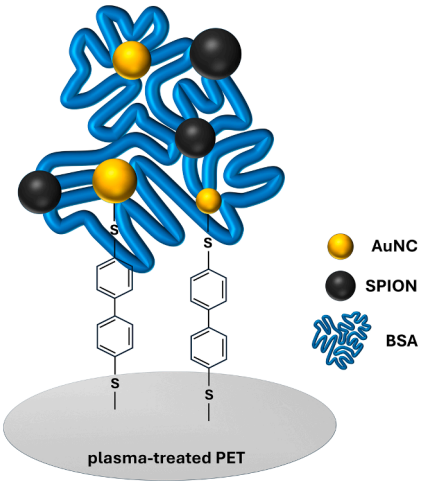

Fig. 4. Schematic depiction of Au-BSA-SPION@pl-BPD-PET, i.e. bimetallic nanocomposite grafted on plasma-treated BPD-modified PET substrate.

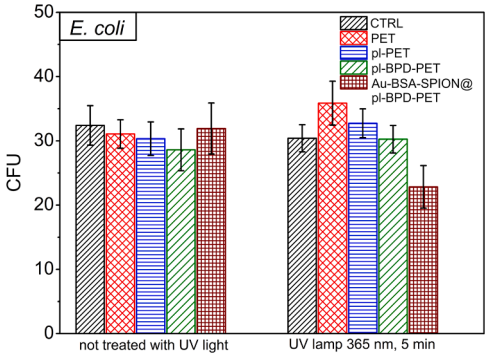

Fig. 5. Results of antibacterial testing of PET substrate, plasma-treated PET substrate, plasma-treated BPD-modified PET substrate, and plasma-treated BPD-modified PET substrate with grafted bimetallic nanocomposites against *Escherichia coli*. Colony forming units (CFU) are expressed on y axis. As a control (CTRL), bacterial suspension was dropped on the bottom of a sterile Petri dish. On the left side of the graph, results obtained under ambient conditions are shown; whereas on the right side of the graph, those obtained upon UVA-light irradiation applied for 5 min.

interaction with the bacteria can be envisaged. As already mentioned in introduction, *E. coli* has been chosen due to its abundance in polluted water. Simultaneously, it has become obvious recently [21] that •OH radicals are efficient in *E. coli* growth inhibition. In our previous work [20], it has been proved (by EPR) that the bimetallic nanocomposites (Au-BSA-SPION) are producing •OH radicals in aqueous environment upon short-time (5 min) UVA light irradiation. Therefore, we wanted to exploit the UVA-light photo-activation of Au-BSA-SPION and, consequent •OH radical formation, to inhibit *E. coli* growth. Therefore, we tested the antibacterial effect against *E. coli* without and with UVA light application as can be compared on left and right parts of Fig. 5, respectively. It should be noted that the graphical representation of bacterial counts (Fig. 5) provides a more reliable basis for interpreting the antibacterial effect, rather than qualitative visual inspection of culture plates. Representative images of the cultivation plates from the antibacterial tests, conducted using the colony-forming unit (CFU) assay, are presented in the Supporting Information (Figure SI-5).

The left part of Fig. 5 shows results of CFU assay performed under standard cultivation conditions. One can conclude from the left part of Fig. 5 that no antibacterial activity is observed in any of the samples (there is mutual similarity considering the appropriate error bars). On the contrary, the right part of Fig. 5 provides results obtained while UVA light (365 nm) irradiation is applied for 5 min. In this case, the previous similarity among the systems with respect to antibacterial properties has significantly disappeared. The comparison of the two sections (left and right) of Fig. 5 reveals two distinguishable qualitative trends: decrease of the average CFU value in the case of control and Au-BSA-SPION@pl-BPD-PET; whereas its increase in the other cases (PET, pl-PET, pl-BPD-PET). The possible reason might be in different wettability of substrates influenced by differences in the extent of UVA radiation impact. Importantly, the decrease of the average CFU value dominated and substantially exceeded the experimental error in the case of bimetallic nanocomposites grafted on surface-modified polymer when comparing left and right parts of Fig. 5.

Therefore, Fig. 5 demonstrates that UVA light (365 nm) applied for 5 min leads to a significant antibacterial effect of bimetallic nanocomposites grafted on modified PET substrate against *E. coli*. Importantly, the antibacterial effect of Au-BSA-SPION@pl-BPD-PET is switch-on by the UVA light solely, thus photo-induced as expected when considering our recent work [20]. In other words, this indicates that inherited nontoxicity of bimetallic nanocomposite (Au-BSA-SPION) that was successfully used as an inert dual imaging probe in vivo [23], can be turned into antibacterial agent against *E. coli* simply by a short-time UVA light irradiation. In fact, such irradiation creates •OH radicals near the substrate surface (at solid-liquid interface) most probably and hence inhibits the growth of *E. coli* (since the control gives evidence that UVA light does not induce *E. coli* growth inhibition – Fig. 5). The direct proof of •OH radical formation has been provided by us using EPR recently for the same bimetallic nanocomposite in aqueous solution [20]. Hence, according to the results summarized in Fig. 5, we speculate that Au-BSA-SPION becomes toxic for *E. coli* most probably due to swift •OH radical formation induced by UVA light applied for 5 min.

It is important to emphasize that a brief UVA radiation exposure (5 min at 365 nm) is required in our case, which is both more economically feasible and practically convenient compared to longer exposure durations. For instance, the prolonged time of 8 h was used in ref [16]. The authors [16] employed 300 nm light to unveil primary amine groups that impart antimicrobial activity to a smart polymer. Similarly, in Ag-Ru-ZnO nanocomposite systems [6], antibacterial properties against *E. coli* were activated by a prolonged UVA-light irradiation. Contrary to these examples, the bimetallic nanocomposites grafted on surface-modified PET substrates did not require such prolonged UVA-light exposures. Due to the nature of Au-BSA-SPION, only short-time UV-light exposure is preferred because prolonged exposure to UV light can cause irreversible changes in the nanocomposite as demonstrated in ref [33].

Owing to grafting to modified PET substrate, Au-BSA-SPION can be easily manipulated to the place of its action, and its photo-switchable antibacterial activity allows for activation at a user-determined time. This holds a promising potential for use as light-activated antibacterial coatings on polymeric substrates. Simultaneously, it can be envisaged that building of bacteria resistance is suppressed because without light-irradiation, the polymeric substrates, plasma-treated surface-modified polymeric substrates, and bimetallic nanocomposite grafted on modified polymeric substrates, all are non-toxic (left part of Fig. 5).

Further work can be devoted to the optimization of PET substrate surface coverage by the bimetallic nanocomposite and to the changes of Au:Fe ratio within the bimetallic nanocomposites to reach higher photo-induced antibacterial impact. It can be also envisaged that our bimetallic nanocomposite could be grafted to other polymeric substrates that need to be surface-modified with the aim of reaching photo-switchable antibacterial properties.

4. Conclusions

Owing to surface properties investigation and spectroscopic characterization of the final system (Au-BSA-SPION@pl-BPD-PET), it was proved that the bimetallic nanocomposite is covalently attached (via Au-

S bond) to the PET surface that has been pre-modified by BPD. This indicates that the bimetallic nanocomposites, where Au–S linkages are utilized, can still form the same bonding type with the surface-modified substrate.

The antibacterial effect of the final system against E. coli was clearly demonstrated to be activated exclusively by a 5-minute UVA light irradiation. This represents a new photo-activable system that could be successfully used in *E. coli* growth regulation.

Data availability

Data will be made available upon reasonable request addressed to the corresponding authors (either to Karolina Siskova, karolina.siskova@upol.cz, or to Alena Reznickova, alena.reznickova@vscht.cz).

CRediT authorship contribution statement

Veronika Lacmanová: Formal analysis, Investigation. **Radek Ostruszka:** Formal analysis, Investigation. **Martin Petr:** Formal analysis, Investigation. **Petr Slepička:** Formal analysis, Investigation. **Filip Průša:** Formal analysis. **Ondřej Kvítek:** Formal analysis, Investigation. **Anna Kutová:** Formal analysis, Investigation. **Alena Řezníčková:** Conceptualization, Methodology, Project administration, Validation, Visualization, Writing – review & editing. **Karolína Šišková:** Conceptualization, Funding acquisition, Methodology, Resources, Supervision, Writing – original draft, Writing – review & editing.

Declaration of competing interest

The authors declare that they have no known competing financial interests or personal relationships that could have appeared to influence the work reported in this paper.

Acknowledgments

Financial support by Czech Science Foundation (project no 25–15590S) and Ministry of Education, Youth and Sports of the Czech Republic (project no LM2023066) is gratefully acknowledged. Hoang Yen Nguyenová is acknowledged for help with revisions and Navami Sunil is thanked for English corrections.

Supplementary materials

Supplementary material associated with this article can be found, in the online version, at doi:10.1016/j.nexres.2025.100996.

References

[1] H. Bai, F. Lv, L. Liu, S. Wang, Supramolecular antibiotic switches: a potential strategy for combating drug resistance, Chem. - Europ. J. 22 (32) (2016) 11114–11121, https://doi.org/10.1002/chem.201600877.
[2] R.J. Turner, The good, the bad, and the ugly of metals as antimicrobials, *BioMetals*. Springer Sci Business Media B.V. (June 1, 2024) 545–559, https://doi.org/10.1007/s10534-023-00565-y.
[3] R. Nudelman, S. Gavriely, D. Bychenko, M. Barzilay, T. Gulakhmedova, E. Gazit, S. Richter, Bio-assisted synthesis of bimetallic nanoparticles featuring antibacterial and photothermal properties for the removal of biofilms, J. Nanobiotechnology. 19 (1) (2021), https://doi.org/10.1186/s12951-021-01183-x.
[4] D. Panchal, S. Pal, Photo-induced synthesis of coral-like hierarchical Ag-Fe bimetallic multifunctional nanostructures, Chem. Mater. 33 (16) (2021) 6501–6513, https://doi.org/10.1021/acs.chemmater.1c01978.
[5] H. Tong, Y. Yang, F. Shi, M. Ding, L. Luo, Y. Miao, Y. Huo, H. Li, Bimetallic CoxCuy-CAT-1 metal-organic frameworks for synergistic antibacterial contribution of photocatalytic-photothermal effect, J. Environ. Chem. Eng. 10 (3) (2022), https://doi.org/10.1016/j.jece.2022.107582.
[6] P.K. Jha, T. Jaidumrong, D. Rokaya, C. Ovatlarnporn, Callistemon Viminalis leaf extract phytochemicals modified silver-ruthenium bimetallic zinc oxide nanocomposite biosynthesis: application on nanocoating photocatalytic *Escherichia coli* disinfection, RSC. Adv. 14 (16) (2024) 11017–11026, https://doi.org/10.1039/d4ra01355g.
[7] T. Wang, X. Fan, R. Li, J. Xu, J. Liu, Multi-enzyme-synergetic ultrathin protein nanosheets display high efficient and switch on/off antibacterial activities, Chem. Eng. J. (2021) 416, https://doi.org/10.1016/j.cej.2021.129082.
[8] Q. Wang, Y. Feng, M. He, Y. Huang, W. Zhao, C. Zhao, Thermoresponsive antibacterial surfaces switching from bacterial adhesion to bacterial repulsion, Macromol. Mater. Eng. (5) (2018) 303, https://doi.org/10.1002/mame.201700590.
[9] J. Xi, J. Zhang, X. Qian, L. An, L. Fan, Using a visible light-triggered PH switch to activate nanozymes for antibacterial treatment, RSC. Adv. 10 (2) (2019) 909–913, https://doi.org/10.1039/c9ra09343e.
[10] S. Perni, C. Piccirillo, A. Kafizas, M. Uppal, J. Pratten, M. Wilson, I.P. Parkin, Antibacterial activity of light-activated silicone containing methylene blue and gold nanoparticles of different sizes, J. Clust. Sci. 21 (3) (2010) 427–438, https://doi.org/10.1007/s10876-010-0319-5.
[11] M. Wegener, M.J. Hansen, A.J.M. Driessen, W. Szymanski, B.L. Feringa, Photocontrol of antibacterial activity: shifting from UV to red light activation, J. Am. Chem. Soc. 139 (49) (2017) 17979–17986, https://doi.org/10.1021/jacs.7b09281.
[12] D. Ci, N. Wang, Y. Xu, S. Wu, J. Wang, H. Li, S. Xuan, Q. Fang, SiO2@AuAg/PDA hybrid nanospheres with photo-thermally enhanced synergistic antibacterial and catalytic activity, RSC. Adv. 14 (7) (2024) 4518–4532, https://doi.org/10.1039/d3ra07607e.
[13] Y. Zheng, X. Cai, G. Chen, D. Xiang, W. Shi, J. Shen, B. Xiang, Single atom-dispersed silver incorporated in ZIF-8-derived porous carbon for enhanced photothermal activity and antibacterial activities, Int. J. Nanomedicine 19 (2024) 4253–4261, https://doi.org/10.2147/IJN.S459176.
[14] A. Khaligh, R. Khan, D.D. Akolpoğlu Başaran, M. Özkan, D. Tuncel, Photoactive catalytically self-threaded 2D polyrotaxane network for visible light activated antimicrobial phototherapy, ACS. Appl. Polym. Mater. 2 (12) (2020) 5726–5734, https://doi.org/10.1021/acsapm.0c01010.
[15] J. Zhao, Y. Li, C. Zhao, Z. Wang, H. Li, Z. Gao, C. Ding, Y.Y. Song, Phospholipid membrane-protected photoelectrochemical chip: a specific test-to-treat platform for bacteria secreting pore-forming toxins with phosphatidylcholine receptor, Chem. Eng. J. (2023) 478, https://doi.org/10.1016/j.cej.2023.147370.
[16] Shao, Z.; Hakobyan, K.; Xu, J.; Chen, R.; Kumar, N.; Willcox, M.; Wong, E.H.H. Photoinduced unveiling of cationic amine: toward smart photoresponsive antimicrobial polymers. *ACS. Appl. Polym. Mater.* 2023, 5 (10), 8735–8743. https://doi.org/10.1021/acsapm.3c01904.
[17] Q. Wang, N. Chen, M. Li, S. Yao, X. Sun, X. Feng, Y. Chen, Light-related activities of metal-based nanoparticles and their implications on dermatological treatment, Drug Deliv. Transl. Res. (February 1, 2023) 386–399, https://doi.org/10.1007/s13346-022-01216-4. Springer.
[18] T. Bayisa, G. Deressa, Z. Feyisa, L. Guta Inki, N.K. Gupta, In-situ synthesis of CuO/TiO2 nanocomposite onto amine modified cotton fabric for antibacterial durability and UV protection, J. Natural Fibers 21 (1) (2024), https://doi.org/10.1080/15440478.2024.2346120.
[19] X. Guo, X. Zhang, M. Yu, Z. Cheng, Y. Feng, B. Chen, Iron decoration in binary graphene oxide and copper Iron sulfide nanocomposites boosting catalytic antibacterial activity in acidic microenvironment against antimicrobial resistance, J. Colloid. Interface Sci. 661 (2024) 802–814, https://doi.org/10.1016/j.jcis.2024.02.019.
[20] G. Zoppellaro, R. Ostruszka, K. Siskova, Engineered protein-iron and/or gold-protein-iron nanocomposites in aqueous solutions upon UVA light: photo-induced electron transfer possibilities and limitations, J. Photochem. Photobiol. a Chem. 2024 (450) (August 2023) 115415, https://doi.org/10.1016/j.jphotochem.2023.115415.
[21] J. Lim, S. Park, S. Ryu, S. Park, M.S. Kim, Different inactivation mechanisms of Staphylococcus Aureus and *Escherichia coli* in water by reactive oxygen and nitrogen species generated from an Argon plasma jet, Environ. Sci. Technol. (2025), https://doi.org/10.1021/acs.est.4c10363.
[22] R. Ostruszka, D. Půlpánová, T. Pluháček, O. Tomanec, P. Novák, D. Jirák, K. Šišková, Facile one-pot green synthesis of magneto-luminescent bimetallic nanocomposites with potential as dual imaging agent, Nanomaterials 13 (6) (2023) 1027, https://doi.org/10.3390/nano13061027.
[23] R. Ostruszka, A. Halili, T. Pluháček, L. Rárová, D. Jirák, K. Šišková, Advanced protein-embedded bimetallic nanocomposite optimized for in vivo fluorescence and magnetic resonance bimodal imaging, J. Colloid. Interface Sci. 663 (2024) 467–477, https://doi.org/10.1016/j.jcis.2024.02.116 (February).
[24] S.K. Paikra, S. Bauri, M. Mishra, Fabrication of nanostructured surfaces towards the prevention of hospital-acquired infection, J. Clust. Sci. (August 1, 2024) 1687–1707, https://doi.org/10.1007/s10876-024-02652-7. Springer.
[25] S.S. Sackey, M.K. Vowotor, A. Owusu, P. Mensah-Amoah, E.T. Tatchie, B. Sefa-Ntiri, C.O. Hood, S.M. Atiemo, Spectroscopic study of UV transparency of some materials, Environ. Pollut. 4 (4) (2015), https://doi.org/10.5539/ep.v4n4p1.
[26] A. Řezníčková, Z. Kolská, V. Hnatowicz, P. Stopka, V. Švorčík, Comparison of glow argon plasma-induced surface changes of thermoplastic polymers, Nucl. Instrum. Methods Phys. Res. B 269 (2) (2011) 83–88, https://doi.org/10.1016/j.nimb.2010.11.018.
[27] V. Švorčík, Z. Kolská, O. Kvítek, J. Siegel, A. Řezníčková, P. Řezanka, K. Záruba, Soft and rigid" dithiols and Au nanoparticles grafting on plasma-treated polyethyleneterephthalate, Nanoscale Res. Lett. 6 (2011) 1–7, https://doi.org/10.1186/1556-276X-6-607.
[28] A. Reznickova, Z. Novotna, Z. Kolska, V. Svorcik, Immobilization of silver nanoparticles on polyethylene terephthalate, Nanoscale Res. Lett. 9 (1) (2014) 1–6, https://doi.org/10.1186/1556-276X-9-305.

[29] H.Y. Nguyenova, B. Vokata, K. Zaruba, J. Siegel, Z. Kolska, V. Svorcik, P. Slepicka, A. Reznickova, Silver nanoparticles grafted onto PET: effect of preparation method on antibacterial activity, React. Funct. Polym. (2019) 145, https://doi.org/10.1016/j.reactfunctpolym.2019.104376.

[30] C.Y. Lim, N.A. Owens, R.D. Wampler, Y. Ying, J.H. Granger, M.D. Porter, M. Takahashi, K. Shimazu, Succinimidyl Ester surface chemistry: implications of the competition between aminolysis and hydrolysis on covalent protein immobilization, Langmuir. 30 (43) (2014) 12868–12878, https://doi.org/10.1021/la503439g.

[31] B. Abada, J. Safarik, K.P. Ishida, S. Chellam, Phenomenological interpretations of membrane properties following repeated chemical cleaning of an end-of-life potable reuse reverse osmosis element dominated by inorganic fouling, ACS ES T Eng. 5 (1) (2025) 167–178, https://doi.org/10.1021/acsestengg.4c00486.

[32] C.F.G. Ferreira, E.M. Benelli, J.J. Klein, W. Schreiner, P.C. Camargo, Effect of protein solution components in the adsorption of Herbaspirillum Seropedicae GlnB protein on Mica, Colloids. Surf. B Biointerfaces. 73 (2) (2009) 289–293, https://doi.org/10.1016/j.colsurfb.2009.05.034.

[33] R. Ostruszka, G. Zoppellaro, O. Tomanec, D. Pinkas, V. Filimonenko, K. Šišková, Evidence of Au(II) and Au(0) states in bovine serum albumin-Au nanoclusters revealed by CW-EPR/LEPR and peculiarities in HR-TEM/STEM imaging, Nanomaterials 12 (9) (2022), https://doi.org/10.3390/nano12091425.